

Effect of spiral vanes width on the separation performance of a hydrocyclone

Peikun Liu, Xiaoguo Wang, Lanyue Jiang, Yuekan Zhang, Xinghua Yang, Xiaoyu Li, Hui Wang

College of Mechanical and Electronic Engineering, Shandong University of Science and Technology, Qingdao 266590, China

Corresponding author: jianglanyue5@163.com (Lanyue Jiang)

Abstract: Aiming at the problem of “entrainment fine particles in underflow” of hydrocyclone in grinding and classification process, a hydrocyclone with spiral vanes (the SV hydrocyclone) was proposed. The CFD techniques were used to study the pressure field, velocity field, turbulence field, particle field and classification efficiency of hydrocyclones with spiral vanes of different widths. The results show that the pressure drop, axial velocity, tangential velocity, turbulence intensity of SV hydrocyclone are reduced in different degrees compared with conventional hydrocyclone, and the reduction becomes more obvious with the increase of vane width. In the case of a vane width of $0.04D$, the underflow recovery rate of $5\mu\text{m}$ and $10\mu\text{m}$ fine particles was reduced by 16.2% and 15.7%. The selection of spiral vanes with small widths is beneficial to improve the separation accuracy of fine particles and reduce the cut particle size.

Keywords: hydrocyclone, vane width, numerical simulation, separation performance

1. Introduction

Hydrocyclone is a device that uses the principle of centrifugal sedimentation to separate the non-uniform phase mixture, with a simple structure, small footprint, and high separation efficiency has been widely used in mineral sorting, metallurgical engineering, petrochemical and sewage treatment industry and many other fields (Song et al., 2020; Xie et al., 2020; Lie et al., 2021; Zhou et al., 2023). However, due to the phenomenon of “entrainment fine particles in underflow” in the hydrocyclone itself, there is the phenomenon of ore over-grinding (Jiang et al., 2020) in the application of grinding and classifying operation, which causes the problems of lower product throughput (Lee et al., 2020) and higher energy consumption (Dundar, 2020), thus increasing the production cost of the coal processing plant. Therefore, the reduction of the “entrainment fine particles in underflow” of hydrocyclone can help save the production cost of coal processing plants to a certain extent.

In response to the problem of reducing underflow entrapment fines in hydrocyclones, many scholars have conducted a lot of research on the structure and performance of the hydrocyclone. Jiang et al. (2022) studied a compound curve cone hydrocyclone, which increases the downward resistance of the fluid and forces the upward migration of the outer vortex fine particles, thus enhancing the quality of the underflow product. Hou et al. (2021) studied a cylindrical-conical hydrocyclone with a flat-bottom conical structure and found that the wide flat-bottom structure increased the cut particle size and reduced the misplacement of fine particles in the underflow. Liu et al. (2023) found that adding a helical structure to the overflow pipe of a hydrocyclone can reduce the pressure drop and explored the optimal location of the helical structure within the hydrocyclone. Qiu et al. (2023) investigated the effects of spiral blade pitch, number of turns and number of heads on the hydrocyclone and obtained an efficiency of 90% and a pressure drop of 0.05 MPa for the hydrocyclone with optimal parameters. Wang et al. (2023) proposed a spiral-wall hydrocyclone, which utilizes the inflow effect of the spiral wall and the enrichment of mineral particles to achieve rapid separation of lead and zinc tailings, in which the recovery of heavy concentrate PbO was increased from 55.55% to 85.25%, which is an increase of nearly

30%. Vysyaraju et al. (2022) designed a new type of hydrocyclone in which a certain number of thin concentric rings were added to the hydrocyclone column and cone sections to reduce the fines bypass. Zhou et al. (2018) examined the effect of the number of guide vane turns on the flow field inside the hydrocyclone separator and showed that increasing the number of turns improved the stability within the hydrocyclone field, resulting in a decrease in both turbulence intensity and pressure drop. Patra et al. (2017) compared spiral rib hydrocyclones with conventional hydrocyclones through experiments and simulations, showing that spiral rib hydrocyclones have lower pressure drop and smaller cut particle size at high inlet velocity conditions. Patra et al. (2018) applied the ribbed hydrocyclone to the process of removing methyl orange from an aqueous solution using fly ash as an adsorbent and analyzed the particle separation performance and dye removal efficiency of this hydrocyclone through experiments. Jung et al. (2019) added a concave and a convex helical configuration to the inner wall of the hydrocyclone, and the classification efficiency of the hydrocyclone being used for asphalt particle separation was investigated by numerical simulation. The classification efficiency of the hydrocyclone with a concave spiral structure was 92.51%, which was 7.41% higher than that of the conventional hydrocyclone.

The flow field inside the hydrocyclone is more complex when it is in operation, so the numerical simulation can provide a more comprehensive understanding and obtain the flow field data (Liu et al., 2020). CFD techniques have been widely used and have gained the recognition of the majority of researchers (Murthy and Bhaskar, 2012; Vega-Garcia et al., 2018; Jing et al., 2021). However, accurate flow field prediction requires the selection of appropriate turbulence models and multiphase flow models, and currently, the more used turbulence models are the Reynolds stress model (RSM) (Ishak and Ayoub, 2019) and the large eddy model (LES) (Padhi et al., 2020). Multi-phase flow models are widely used, such as the Volume of Fluid (VOF) model (Mokni et al., 2015), Mixture model (Su and Zhang, 2022), and Euler model (Zhang and Ni, 2022). Yang et al. (2022) applied RSM and VOF models to simulate the flow field of continuous hydrocyclones, introduced the DPM model to track the particle trajectories, and conducted experimental investigations. Ye et al. (2022) and Hou et al. (2021) used RSM and two-fluid model (TFM) to simulate the flow field and classification efficiency inside the hydrocyclone, and verified the feasibility of the method. Xing et al. (2022) apply the population balance model (PBM) to the continuity equation for hydrocyclone simulation based on the Euler-Euler method and verifies the correctness of the simulation by particle image velocimetry. Je et al. (2022) adopted Mixture and RSM models for numerical calculations of axial flow separators, and the neural network model for predicting separation performance showed better variance than the multilinear regression model (MLR). Vakamalla and Mangadoddy (2019) used Mixture model and LES to explore the development of 250 mm hydrocyclone air core and particle distribution, and the flow field was verified by laser Doppler velocimetry, and the predicted particle distribution curves were in good agreement with the experimental data. Zhao et al. (2022) used the Mixture multiphase flow model to simulate the flow field and separation efficiency inside the hydrocyclone, and verified the accuracy of the numerical calculation results through experiments. Padhi et al. (2019) used the Mixture model to simulate the classification efficiency of multiple components within the hydrocyclone and showed that the simulation and the test were in general agreement. Su and Zhang (2022) adopted RSM, VOF, and Mixture models to predict the hydrocyclone separation process, and explored the effects of vortex finder and feed parameters on short-circuit flow and classification efficiency using experiments and simulations. Kou et al. (2022) used a combination of RSM and Mixture to simulate the two-phase flow, and the simulation results were in good agreement with the experimental results. However, in the selection of the turbulence model, the LES model requires higher computer performance, which can lead to longer computation time, so the RSM turbulence model was selected for the hydrocyclone simulation.

From the research of experts and scholars, it is revealed that spiral vanes can improve the flow field of hydrocyclone to a certain extent, but the influence law of spiral vanes width on hydrocyclone flow field and separation performance is not clear.

Therefore, in this paper, a hydrocyclone with spiral vanes is studied, and six types of spiral vanes with different widths are designed, and the width of these spiral vanes is proportional to the diameter

of the hydrocyclone. CFD technology is used to investigate the effect of the width of the spiral vanes on the flow field and separation performance in the hydrocyclone by numerical simulation.

2. Model and method geometry

2.1. Geometric structure

The spiral vanes are fixed on the inner wall of the hydrocyclone, and under the action of the centrifugal force field of the hydrocyclone, the mixed fluid is thrown to the wall along the direction of the spiral vane movement. To investigate the influence of the width of the spiral vanes on the hydrocyclone, a hydrocyclone model is established as shown in Fig. 1. The center of the spigot is determined as the origin, the inlet port is along the positive direction of the Y-axis, and the overflow pipe is along the positive direction of the Z-axis. The characteristic height $Z=233\text{mm}$ and $Z=170\text{mm}$ were selected as the cross sections for comparative analysis. In this paper, considering that the spiral vanes are mainly added at the position of the column section of the hydrocyclone, the selection of the width of the vanes is based on the radial distance between the inner wall surface of the hydrocyclone and the outer wall of the vortex finder. The ratio of vane width to hydrocyclone diameter (C/D) was defined as x . Six different widths of spiral vanes were designed with ratios (C/D) of 0.04, 0.08, 0.12, 0.16, 0.20, and 0.24. The structural parameters of the hydrocyclone are shown in Table 1, because of the spiral vanes fixed on the wall of the hydrocyclone, it is named as hydrocyclone with spiral vanes, abbreviated as SV hydrocyclone.

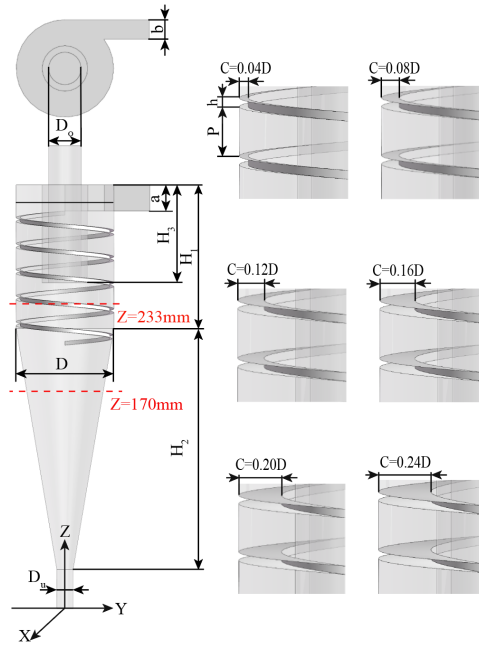


Fig. 1. Structural parameters of hydrocyclones

Table 1. Structural dimensions of the hydrocyclone

Structure parameters	Size
Body diameter D/mm	75
Size of inlet $a \times b/\text{mm}$	20×15
Height of cylinder section H_1/mm	110
Height of cone section H_2/mm	185
Height of inner vortex finder H_3/mm	75
Diameter of overflow D_o/mm	25
Diameter of spigot D_u/mm	12.5
Height of vanes h/mm	3
Width of vanes C/mm	xD
Pitch of vanes P/mm	20

2.2. Model description

The RSM turbulence model accurately predicts the Reynolds stress and anisotropy of the complex flow field. Due to the fast flow velocity and high turbulence intensity in the internal flow field of the hydrocyclone, the RSM model is often used in the numerical simulation of the hydrocyclone. In this study, firstly, the flow field data of the hydrocyclone are obtained by VOF model and RSM model, and the pressure field, velocity field, and turbulence field are analyzed. Then the Mixture model combined with RSM model was used to obtain particle phase data and compare the results of the effect of spiral vanes with different sizes and widths on particle classification.

The Reynolds stress transport equation can be written as:

$$\frac{\partial(\overline{\rho u_i' u_j'})}{\partial t} + \frac{\partial(\rho u_k \overline{u_i' u_j'})}{\partial x_k} = D_{T,ij} + D_{L,ij} + P_{ij} + G_{ij} + \phi_{ij} + \varepsilon_{ij} + F_{ij} \quad (1)$$

where $\overline{\rho u_i' u_j'}$ denotes the average Reynolds stress; $D_{T,ij}$ denotes the turbulent diffusion term; $D_{L,ij}$ denotes the molecular viscosity diffusion term; P_{ij} denotes stress-generating term; G_{ij} denotes Buoyancy-generating term; ϕ_{ij} denotes the Stress-strain term; ε_{ij} denotes the viscosity dissipation term; F_{ij} denotes the fluid rotation-generating term; ρ 、 u_k denotes the density and viscosity of the fluid.

The VOF model is suitable for the solution of two-phase or multi-phase fluids that are mutually immiscible. Based on this property, the simulated gas-liquid two-phase flow inside the hydrocyclone is studied, and the velocity field characteristics obtained are in good agreement with the LDV measurement results (Zhang et al., 2016). The simulated fluid domain is filled with each phase of fluid and the size of the control volume occupied by each phase of fluid is the volume fraction of this simulated fluid domain and the sum is 1.

$$\sum_{q=1}^n \alpha_q = 1 \quad (2)$$

where α_q is the volume fraction of the q-phase fluid.

The Mixture model predicts the discrete phase through the mixed-term momentum equation with the continuity equation. It can describe the flow field distribution of the mixing action of multiphase fluids, and the accuracy of the model has been verified by many scholars (Zhao et al., 2022; Padhi et al., 2019).

The continuous equation is expressed as follows:

$$\frac{\partial}{\partial t}(\rho_m) + \nabla \cdot (\rho_m \vec{v}_m) = 0 \quad (3)$$

The momentum equation of the Mixture model is expressed as follows:

$$\frac{\partial}{\partial t}(\rho_m \vec{v}_m) + \nabla(\rho_m \vec{v}_m \vec{v}_m) = -\nabla \cdot \vec{p} + \nabla \cdot [\mu_m(\nabla v_m + \nabla \vec{v}_m^T)] + \rho_m \vec{g} + \vec{F} + \nabla \cdot (\sum_{k=1}^N \alpha_k \rho_k \vec{v}_k^r \vec{v}_k^r) \quad (4)$$

where ρ_m is the density of the mixed phase; \vec{v}_m is the average mass velocity; \vec{p} is the pressure; \vec{F} is the volume force; μ_m is the viscosity of the mixed phase; ρ_k is the density of the k-phase; N is the number of phases; v_k^r represents the slip velocity of the phase k relative to the mixed phase.

The particle motion equation can be written in the following form:

$$\frac{d\vec{u}_p}{dt} = f_D(\vec{u} - \vec{u}_p) + \frac{\vec{g}_x(\rho_p - \rho)}{\rho_p} + \vec{F} \quad (5)$$

where \vec{F} is an additional force; $f_D(\vec{u} - \vec{u}_p)$ is the drag force per unit particle mass.

$$f_D = \frac{18\mu}{\rho_p d_p^2} \frac{C_p R_e}{24} \quad (6)$$

where \vec{u}_p is particle velocity; \vec{u} is fluid velocity; ρ_p is particle density; ρ is fluid density; \vec{g}_x is the acceleration of gravity in the x-direction; μ is molecular viscosity of the fluid; d_p is particle size; C_p is drag coefficient; R_e is relative Reynolds number, which can be written as

$$R_e = \frac{\rho d_p (\vec{u} - \vec{u}_p)}{\mu} \quad (7)$$

2.3. Simulation conditions

As shown in Fig. 1, the model structure of the SV hydrocyclone is relatively complex, and the tetrahedral mesh has better adaptability to the more complex geometry structure (Duczek et al., 2016; Zhang and

Qian, 2012). Therefore, tetrahedral meshing is used to mesh the model in this simulation. The number of grids will have an impact on the model prediction results; too small several grids will affect the calculation accuracy, and too many will prolong the simulation calculation time. Therefore, the number of grids should be controlled within a suitable range under the condition of maintaining computational accuracy. When the width of the spiral vane is $0.04D$, the grid number of hydrocyclone is divided into 163824, 243259, 318294, 389596, and 481254, and the tangential velocity value at the axial height $Z=230\text{mm}$ is used as the basis of grid independence verification. As seen in Fig. 2(a), the tangential velocity of the hydrocyclone remains constant after the number of grids is greater than 318294.

The overall mesh and the spiral vanes mesh are shown in Fig. 2(b), and the spiral vanes are mesh encrypted to improve the calculation accuracy. The Y^+ values of the hydrocyclone wall in Fig. 2(c) are between 20 and 254, which ensures the accuracy of the model simulation. Finally, the number of grids for the six SV hydrocyclones was determined as 389596, 385369, 379759, 372805, 366795, and 358775. The minor changes in the number of grids were mainly caused by changes in the structure of the spiral vanes.

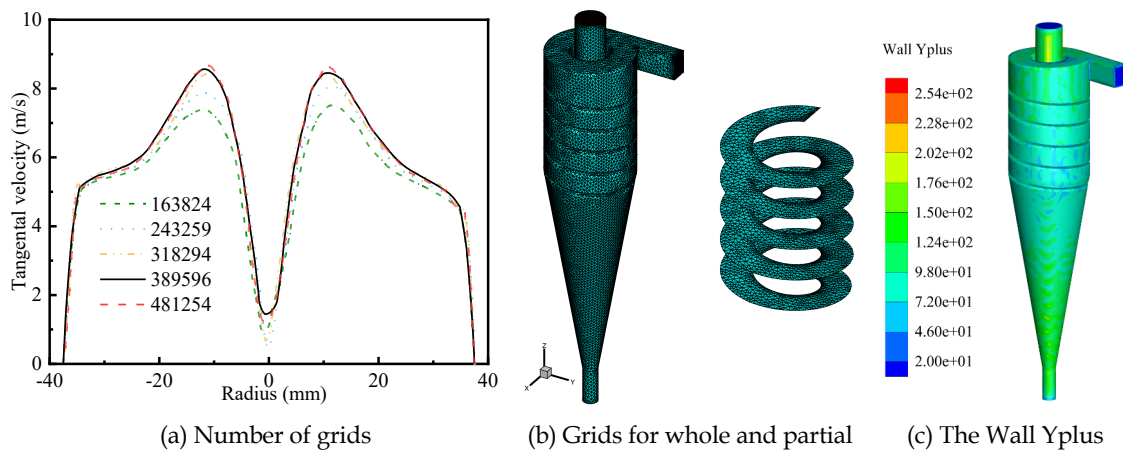


Fig. 2. Hydrocyclone grid validation

In the simulation process using the VOF model, the hydrocyclone inlet boundary condition was set to "velocity inlet" with an inlet velocity of 5m/s ; the boundary conditions of the underflow and overflow ports were set to "pressure outlet"; the air phase return volume fraction is set to 1, and the transient solution is used. In the Mixture model, quartz sand with a 2650 kg/m^3 density was used as the material. Eight different particle sizes were selected, and the particle sizes are shown in Table 3, and the total volume fraction of solids was converted to 3.17% according to the mass concentration of 8%, while the air phase was added to simulate the actual hydrocyclone working conditions. The boundary condition of the hydrocyclone wall is "No Slip". The pressure-velocity coupling is performed using the "SIMPLE" algorithm, with the pressure discretization in the format "PRESTO!" (Tian et al., 2020) and the momentum discretization in the format "QUICK" (Tian et al., 2020). The time step is set to 1.0×10^{-4} and the equilibrium of the mass flow of each phase at the inlet and outlet is used as the convergence condition (Kuang et al., 2012).

Table 2. Particle size distribution

Mean size/ μm	Yield / %	Volume fraction / %
5	9.80	0.310
10	5.48	0.174
20	12.60	0.399
30	12.54	0.398
40	13.23	0.419
60	21.28	0.675
80	16.48	0.523
90	8.59	0.272

3. Results and discussion

3.1. Model validation

In 1988, Hsieh and Rajamani (1988) analyzed the velocity distribution in the characteristic height section of a 75 mm hydrocyclone using LDV. Therefore, before applying to the numerical research work, a three-dimensional model of the 75 mm hydrocyclone was built and the simulation results of the VOF model flow field were compared with the experimental results of Hsieh. Fig. 3 shows the simulated and experimental comparison of tangential and axial velocities in the hydrocyclone flow field with the hydrocyclone classification efficiency. As shown in Fig. 3(a) and Fig. 3(b), the air core is shown in the figure, while the characteristic position is selected as the axial velocity and tangential velocity at 60 mm downward of the hydrocyclone top cover as the evaluation basis, and the simulation results obtained from the gas-liquid two-phase flow inside the hydrocyclone simulated by the VOF model are in basic agreement with the experimental results. The differences revealed at the maximum value of the tangential velocity are mainly caused by the practical application of the model and experimental errors. Figure 3(c) shows the comparison of the grade efficiency curves of the simulated and experimental results, both of which have the same variation trend. Therefore, the comparative analysis of the data can verify the reliability of the turbulence model and multiphase flow model selected for this simulation.

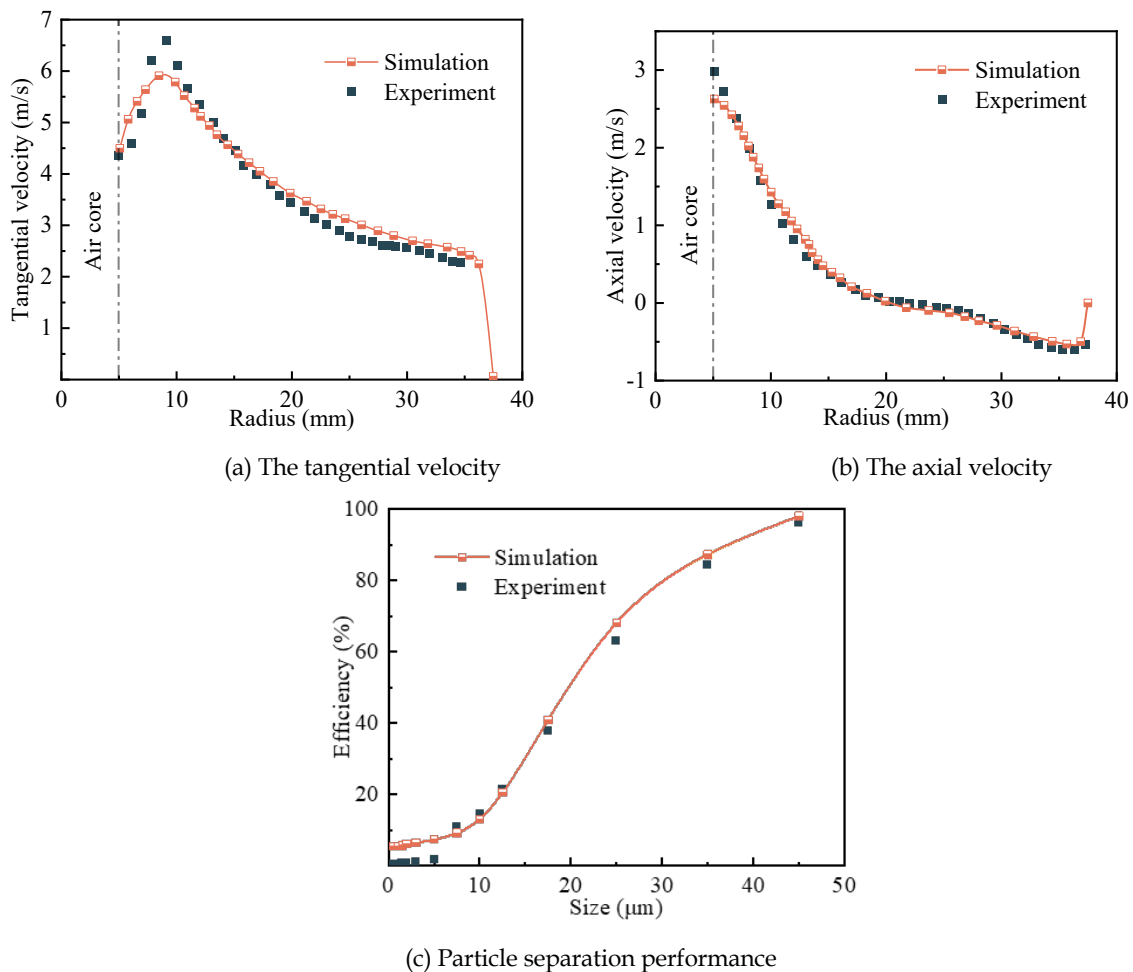


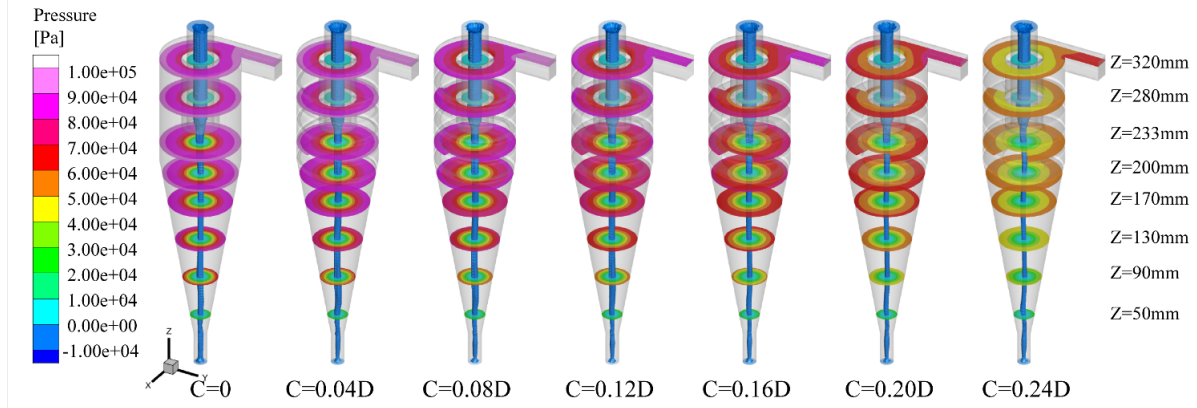
Fig. 3. Validation of the model

3.2. Fluid flow field

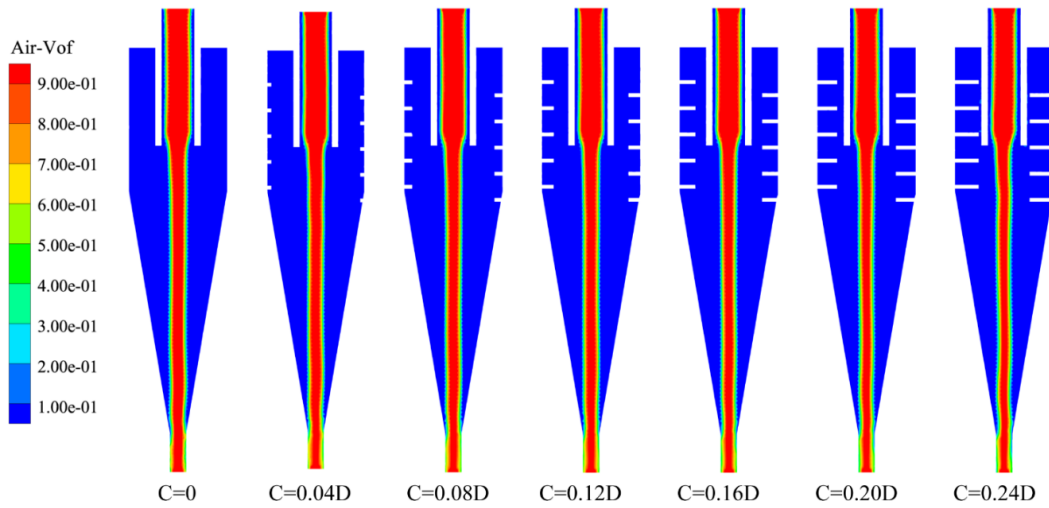
3.2.1. Pressure

Static pressure is one of the important parameters for hydrocyclone operation. Fig. 4(a) and Fig. 4(b) shows the cross-sectional pressure distribution clouds and air core distribution clouds of conventional hydrocyclone and SV hydrocyclone of different widths. In Fig. 4(a) can be obtained in the center section

of the pressure distribution still maintains a good symmetry, indicating that the radial pressure distribution pattern within the flow field of hydrocyclone is not affected by the width of the spiral vanes, and the pressure distribution along the axial position of the same hydrocyclone does not change significantly. The blue column-shaped inner area at the center of Fig. 4(a) is the negative pressure area within the hydrocyclone flow field. The underflow and overflow port of the hydrocyclone are connected with the atmosphere to form the air return flow, and through the negative pressure area to form the air core, which is as shown in the air core contours diagram of Fig. 4(b).



(a) Contours of the pressure distributions



(b) Air core

Fig. 4. Contours of the pressure distributions and air core

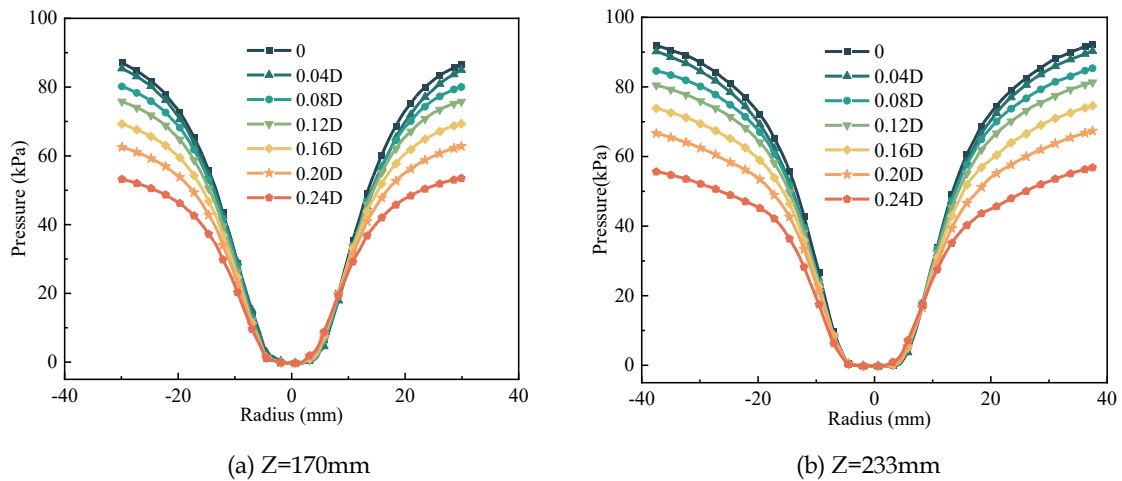


Fig. 5. Comparison of the radial pressure distributions

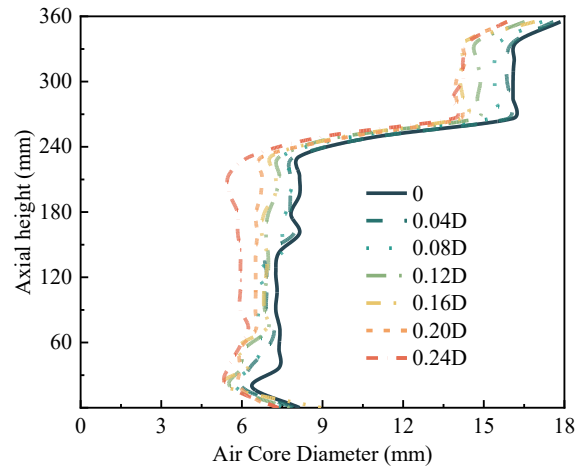


Fig. 6. Comparison of air core diameters

To accurately analyze the effect of the spiral vanes on the static pressure within the flow field of the hydrocyclone, two characteristic heights of axial height $Z=170$ and $Z=233$ mm were selected for analysis. As in Fig. 5(a) and Fig. 5(b), the hydrocyclone static pressure from the wall to the center of the radial decreasing trend, in the vicinity of the air core due to the transformation of pressure energy into kinetic energy resulting in a sharp decrease in pressure gradient, the internal pressure continues to decrease until the formation of negative pressure. In addition, the static pressure inside the hydrocyclone increases with the increase of the spiral vane width. At the vane width $C=0.04D$, the wall static pressure value of SV hydrocyclone decreases by 1.95% and 2.04% respectively compared with the conventional hydrocyclone at two characteristic heights. The main reason is that the hydrocyclone vanes guide the vortex motion of the fluid in the hydrocyclone and reduce the disturbance of secondary vortices in the flow field. Fig. 6 shows the comparison of air core diameter. The air column is the area where the volume fraction of gas in the flow field of the hydrocyclone is greater than 0.9. The air core has a protuberance resembling the Adam's apple that appeared in the overflow pipe area, which is caused by the gas returning from the overflow pipe intersecting with the working fluid here, causing the air core to expand outward. And as the width of the spiral vane increases, the diameter of the air core in the hydrocyclone decreases, and this result is conducive to increasing the hydrocyclone separation area and improving the hydrocyclone processing capacity.

The operation process of hydrocyclone is accompanied by a certain pressure loss, pressure drop refers to the pressure difference between the hydrocyclone inlet pressure and the overflow pipe outlet, which is an important indicator reflecting the energy consumption of hydrocyclone. Fig. 7 shows the hydrocyclone pressure drop diagram, and the scale factor shown is the ratio of the spiral vane width (C) to the hydrocyclone cylinder diameter (D). In the figure, the pressure drop of the hydrocyclone tends to decrease with the increase of the spiral vane width. When the width of spiral vane is $C=0.04D$, the pressure drop of SV hydrocyclone is reduced by 4.04% compared with conventional hydrocyclone, and the pressure drop is the smallest when the width of vane $C=0.24D$, which is reduced by 38.44%. This is due to the addition of a spiral vane makes the diameter of the air core in the hydrocyclone reduced, reducing the kinetic energy required to lose gas in the air core, thus reducing the hydrocyclone energy loss, which can be derived from the introduction of a certain width of the spiral vane can reduce the pressure drop of the hydrocyclone.

Tangential velocity is an important factor to measure the separation performance of hydrocyclones and determines the strength of the centrifugal force field inside the hydrocyclone. Fig. 8 shows the tangential velocity distribution contours of conventional hydrocyclones and SV hydrocyclones of different widths. It can be seen that the tangential velocity in the hydrocyclone also shows a symmetric distribution, from the center point along the radial direction first increases sharply, reaching a maximum near the radial position $r = 12.5$ mm. After that, it gradually decreases with the increase of radial position, and finally drops to zero rapidly near the wall, which obeys the velocity distribution law of the combined vortex.

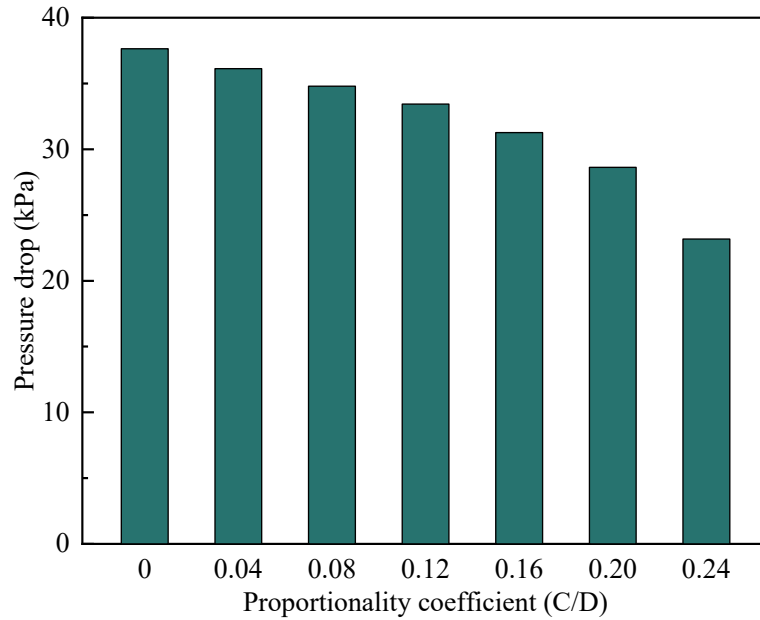


Fig. 7. Pressure drop

3.2.2. Tangential velocity

As shown in Fig. 9(a) and Fig. 9(b), the tangential velocity distribution curves at the position of section height $Z=170$ and $Z=233$ are shown. Compared with the conventional hydrocyclone, the effect on the tangential velocity in the hydrocyclone is not obvious when the width of the spiral vane is $C=0.04D$. As shown in Fig. 9, the overall tangential velocity of the hydrocyclone gradually decreases with the increase of the width of the spiral vanes. The smaller tangential velocity will help to reduce the wall friction and reduce the wear of the inner wall of the hydrocyclone, but it will reduce the centrifugal force field in the flow field of the hydrocyclone and affect the separation efficiency. Because when the width of the spiral vane is too large, the friction generated by the mixed fluid and the spiral vane will be non-negligible, resulting in the loss of fluid kinetic energy. However, the separation of particles is mainly affected by the radial centrifugal force, when the tangential velocity is too low, it will also lead to the coarser particles in the hydrocyclone still located in the inner swirling flow of hydrocyclone, discharged from the vortex finder, resulting in misplaced particles overflow, reducing the separation accuracy. Therefore, the width of the spiral vane should not be too large.

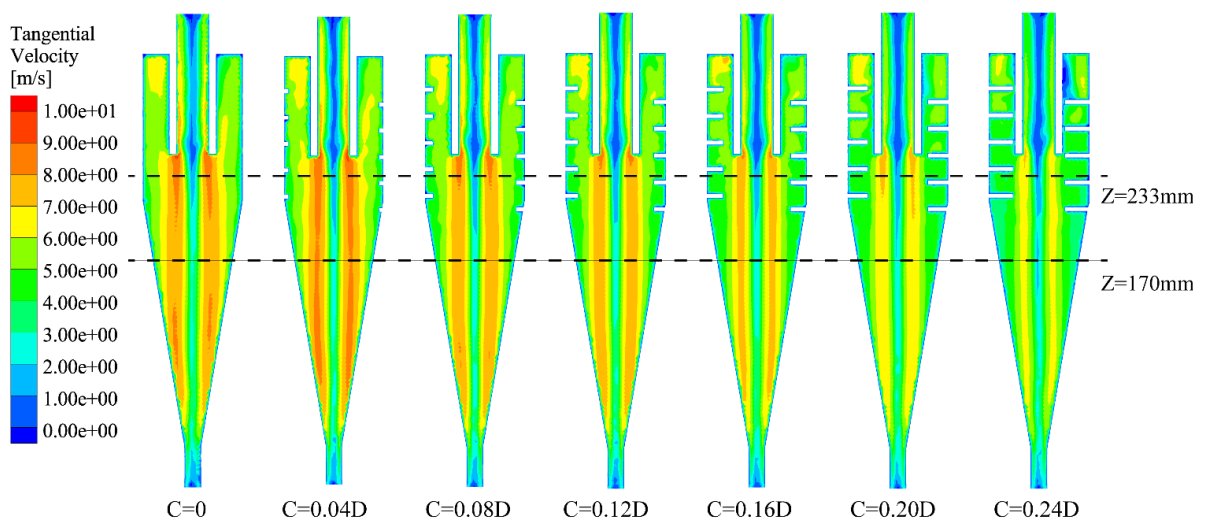


Fig. 8. Contours of the tangential velocity distributions

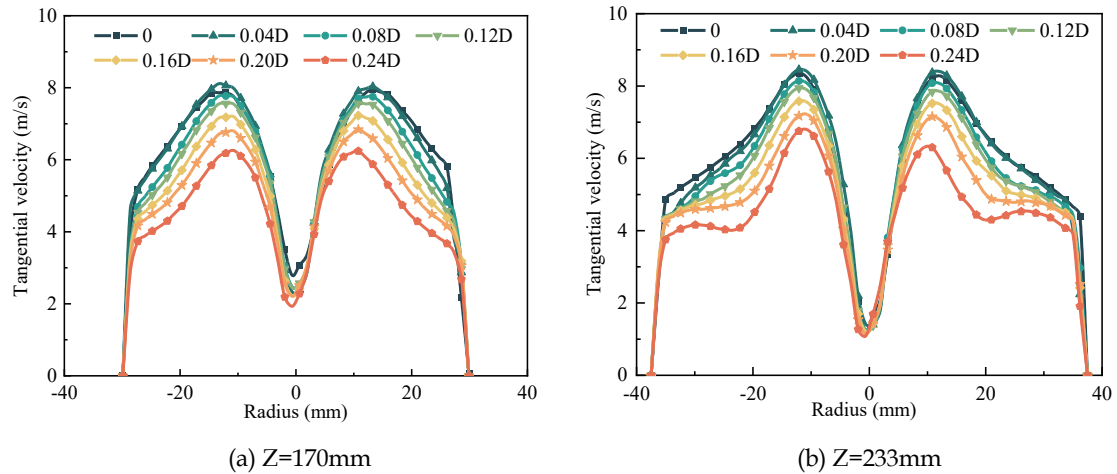


Fig. 9. Comparison of the tangential velocity distributions.

3.2.3. Axial velocity

The axial velocity determines the residence time of particles in the hydrocyclone, which is one of the important indicators to evaluate the separation performance of hydrocyclone. Fig. 10 shows the axial velocity distribution contours of SV hydrocyclone with different widths. The solid black line in the figure represents the line with zero axial velocity in the cross-section (LZVV), which is more seriously distorted in the hydrocyclone column section due to the existence of short-circuit flow and circulating flow, and is not symmetrical in the radial direction and has an inverted cone shape in the cone section. At the same time, LZVV divides the flow field into two regions: the dividing line between the inner and outer swirling flow in the radial direction. The closed black solid line under the cover in the figure indicates the presence of circulating flow in the flow field.

Fig. 11(a) and Fig. 11(b) show the cross-section's velocity distribution at two characteristic height positions. The axial velocity has a clear turn from the wall surface to the central axis, and the axial velocity in the outer swirling flow area of the hydrocyclone gradually decreases as the width of the spiral vanes increases. The reason is that the guide vane has a certain support effect on the fluid in the hydrocyclone, so that the outer swirling flow area working fluid flow along the specified trajectory, smaller axial velocity is conducive to extending the separation time of the particles in the hydrocyclone so that the separation is more adequate. However, increasing the width of the spiral vane causes the flow of outer swirling flow of the hydrocyclone to increase, and this increase will be more likely to aggravate the "entrainment fine particles in underflow" phenomenon.

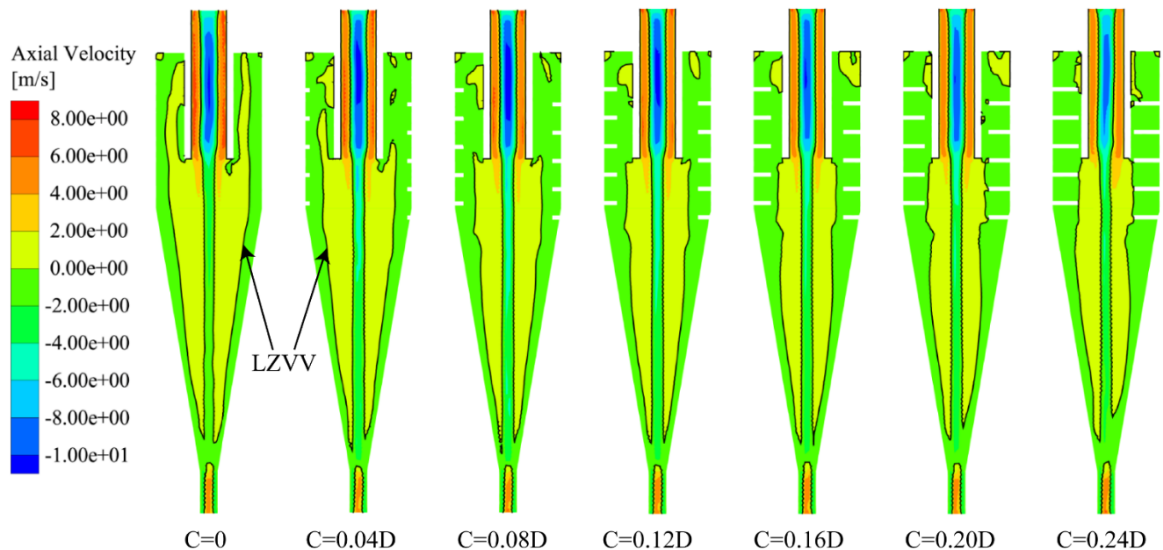


Fig. 10. Contours of the axial velocity distributions

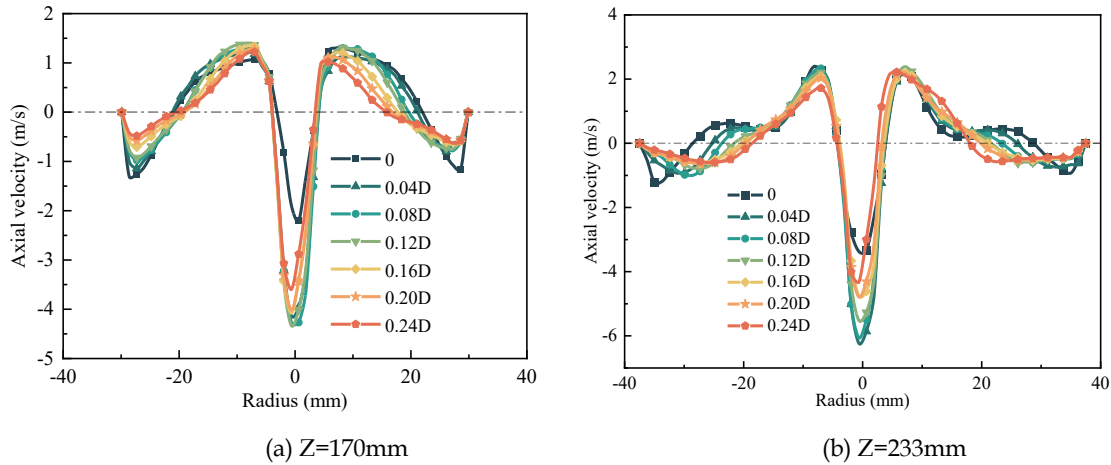


Fig. 11. Comparison of the axial velocity distributions

According to Fig. 12, it can be seen that the variation in the width of the spiral vanes affects the underflow product concentration. At the vane width of $C=0.04D$, the underflow split ratio of SV hydrocyclone increases by 6% and the underflow product concentration decreases by 5.74% compared with the conventional hydrocyclone. Moreover, the increase of the spiral vane width improves the inflow effect, leading to the further increase of the underflow split ratio and the continuous decrease of the underflow product concentration. There are two main reasons to explain this, on the one hand, the spiral vanes make the vortex motion in the hydrocyclone smoother, reducing the turbulence intensity in the flow field, and leading to an increase in the underflow split ratio. On the other hand, the spiral vanes affect the tangential velocity in the hydrocyclone flow field, resulting in a change in the centrifugal force field, which may make the migration of coarse particles in the hydrocyclone to the overflow, resulting in a decrease in the underflow product concentration.

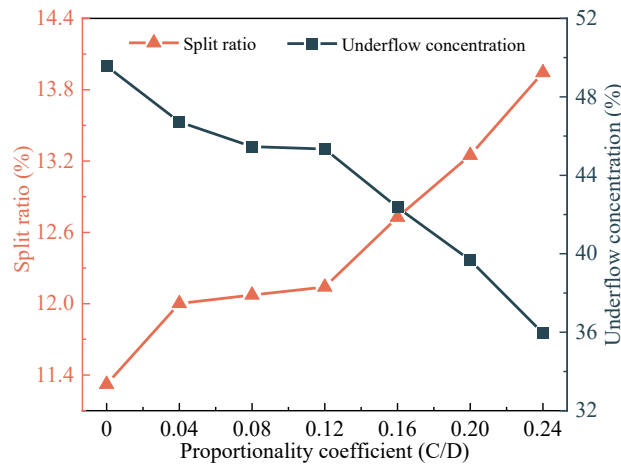


Fig. 12. The underflow split ratio and underflow concentration

3.2.4. Turbulent intensity

The flow field inside the hydrocyclone is a highly complex nonlinear flow field, and the turbulence intensity is commonly used to characterise the strength of the turbulent motion, the size of which affects the stability of the flow field. Fig. 13 shows a contour diagram of the turbulence intensity distribution within the flow field of the SV hydrocyclone, which is mainly selected from the region where the spiral vanes are added. The turbulence field in the figure has certain symmetrical characteristics, and the turbulence intensity in the lower region of the overflow pipe decreases gradually with the increase of the width of the spiral vane. The reason is that the addition of spiral vanes in the hydrocyclone has a certain effect on the flow field, so the flow field in the hydrocyclone is more stable, and this result

reduces the misalignment of particles overflow at the overflow. The maximum turbulence intensity in the hydrocyclone occurs in the region of the overflow pipe, which is mainly caused by the convergence of multiple flows due to the intake of air from the overflow.

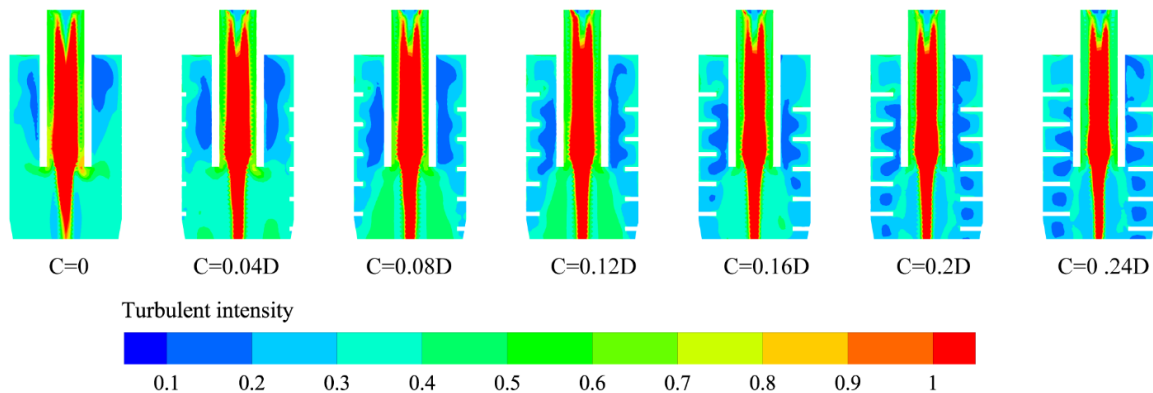


Fig. 13. Contours of the turbulent intensity distributions

3.3. Particle size analysis

3.3.1. Particle volume fraction

Fig. 14 shows the volume distribution contours of different particle sizes, the distribution of different particle sizes in the hydrocyclone flow field varies. Fig. 14(a) and Fig. 14(b) shows the volume distribution contours of the relatively small 5 μm and 10 μm particles in the material, and the white area not shown in the center of the figure represents the air core region. It can be found that the fine particles are mainly distributed near the air core, and the larger the particle size is, the closer the distribution area is to the hydrocyclone wall. The volume fraction content of fine particles in the inner swirling region of SV hydrocyclone ($C=0.04D$) is higher than that of the conventional hydrocyclone, and the volume fraction of fine particles near the bottom end of the cone section is even lower. With the increase of the spiral vane width, the area of the high concentration region of the column section decreases, the position gradually shifts downward, and the fine particles have a tendency to move toward the underflow, increasing the fine particle content of the underflow products. This is because the working fluid in the hydrocyclone and the spiral vane surface friction exists, producing a certain resistance, and the coarse particles have a higher specific gravity, so the resistance effect on fine particles is more obvious. However, the centrifugal force in the particle classification has been dominant in the hydrocyclone, when the spiral blade width is too large, the tangential velocity in the hydrocyclone flow field is obviously reduced, resulting in a weakening of the centrifugal force, so that coarse and fine particles are discharged from the underflow port together.

As can be seen from Fig. 14(c), the 30 μm particles in the hydrocyclone are mainly enriched near the underflow port, and the addition of spiral vanes on the wall has a certain inflow effect on the particles, which improves the underflow recovery performance of the hydrocyclone for coarse particles. However, in the case of a vane width greater than 0.12D, 30 μm particles tend to gather to the overflow port, especially obvious when the vane width is 0.24D, which leads to a reduction in the particle content at the bottom of the hydrocyclone. On the one hand, because the vane width is too large, the spiral vane in the bottom area of the vortex finder will cause the particles to directly enter the overflow, aggravating the hydrocyclone "overflow with coarse particles". On the other hand, the reduction of tangential velocity in the hydrocyclone also causes the coarse particles to move towards the inner swirling flow region. These are the reasons for the reduced recovery of the particle underflow in the hydrocyclone.

3.3.2. Separation performance

The classification efficiency curve is constructed by using the underflow recovery rate of different size particles to reflect the influence of spiral vanes on the classification efficiency of hydrocyclone. Fig. 15

shows the classification efficiency curves of conventional hydrocyclone and SV hydrocyclone. As can be seen from the figure, the underflow recovery rate increases continuously with the increase of particle size, and the classification efficiency curve shifts to the right with the increase of spiral vane width. When the width of spiral vane is 0.04D, the underflow recovery rate of 5 μm and 10 μm fine particles decreases by 16.2% and 15.7%. As the width of the spiral vane increases from 0.04D to 0.24D, the

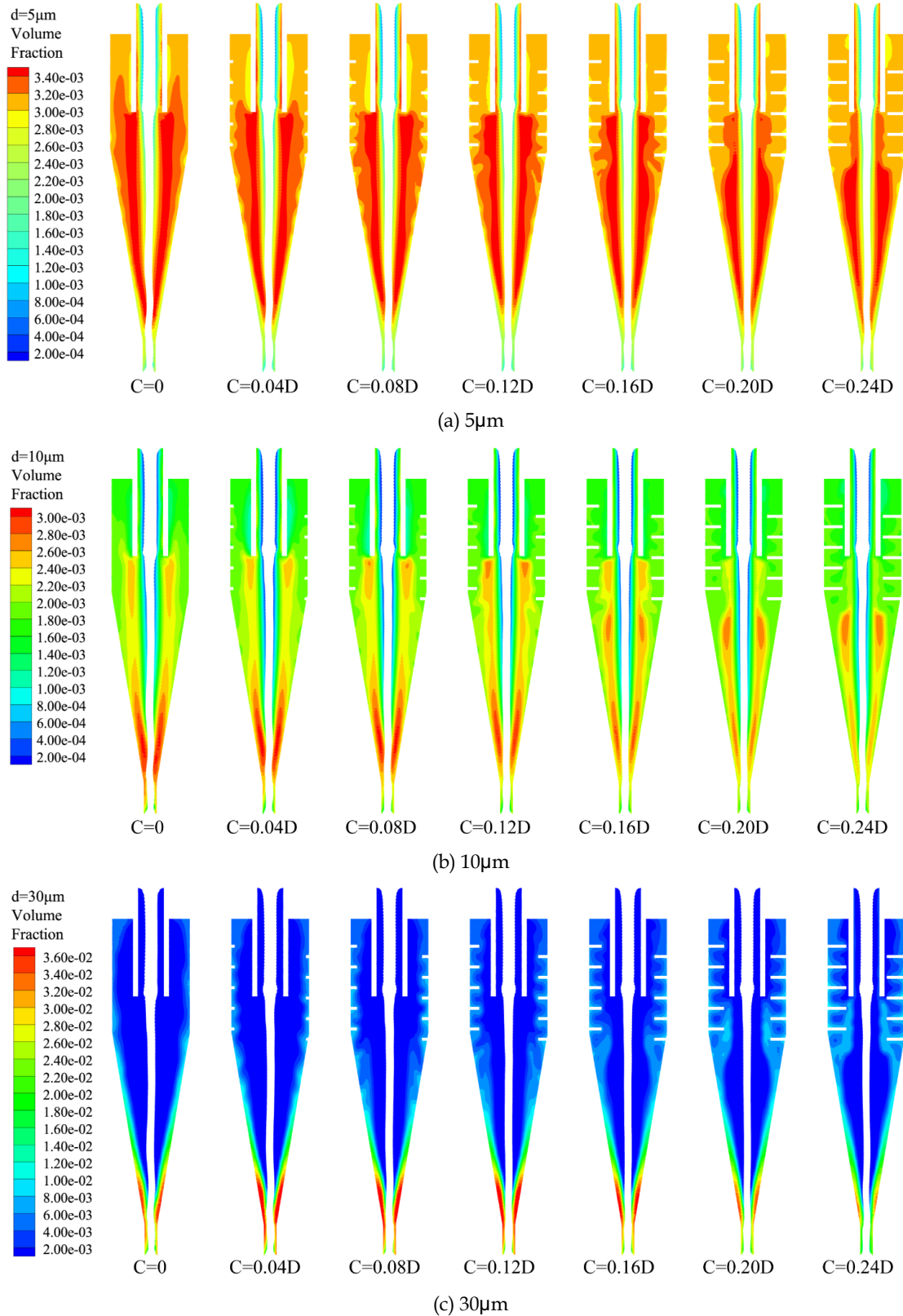


Fig. 14. Contours of particle volume fraction distributions

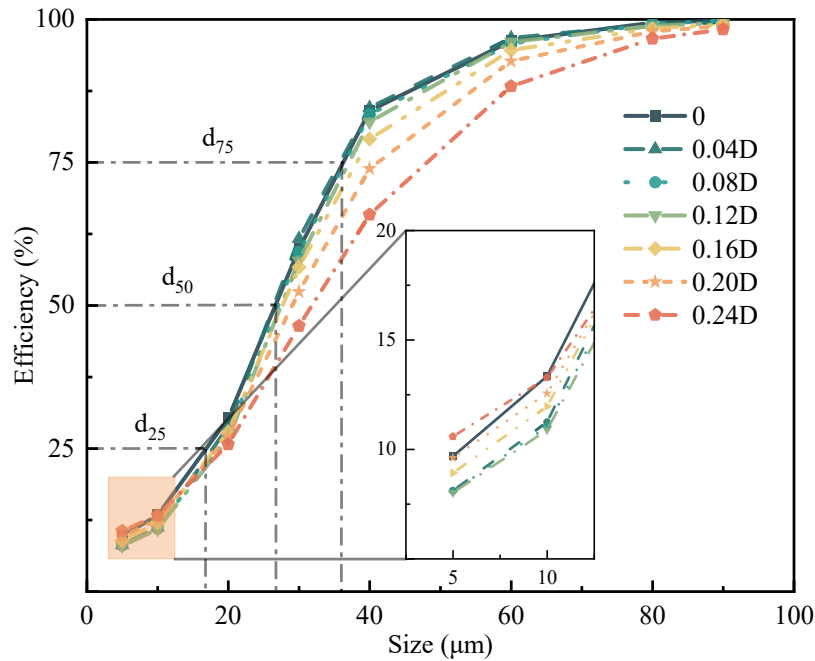


Fig. 15. Recovery rate of particles in the underflow

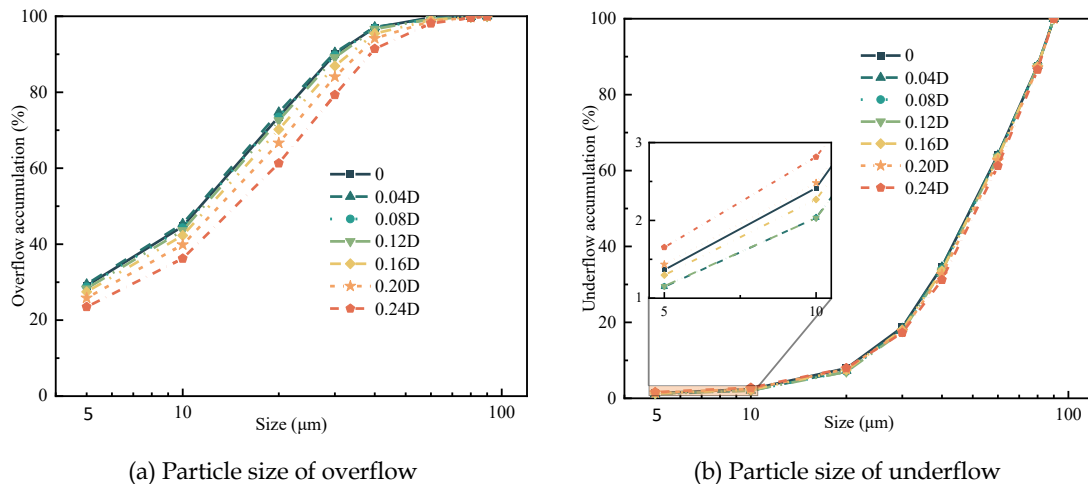


Fig. 16. The particle size of the products

recovery rate of fine particles in the underflow decreases and then increases. At the width of the spiral vane $C=0.12D$, the underflow recovery of fine particles of $5\ \mu\text{m}$ and $10\ \mu\text{m}$ is the smallest. The main reason for this is explained in the particle volume fraction analysis, not to repeat. In addition, increasing the spiral vane width will reduce the diameter of the air core in the hydrocyclone flow field, leading to an increase in the flow of the inner cyclone, more particles from the overflow outflow, will also lead to reduce the content of fine particles in the underflow. However, as the spiral vane width continues to increase, the influence of the centrifugal force field in the hydrocyclone on the particle classification performance gradually increases, too small tangential velocity can not provide sufficient centrifugal force so the hydrocyclone separation performance is reduced.

Fig. 16(a) and Fig. 16(b) show the particle size distribution curves of the overflow product and the underflow product. With the increase of spiral vane width, the cumulative curve of overflow products shifted to the right as a whole, indicating that the content of overflow fine particles gradually decreased. The content of particles below $10\ \mu\text{m}$ in the underflow product decreases first and then increases with the increase of vane width, reaching the lowest at the vane width $C=0.12D$. From the analysis results,

the width of the spiral vane is too large and is not conducive to the classification of fine particles, should be based on the actual working conditions to choose the appropriate width of the spiral vane.

The classification efficiency of the corresponding particles was obtained according to the classification efficiency curve in Fig. 14. The separation performance of the hydrocyclone is evaluated by the indexes of imperfection I, separation sharpness S, and possible deviation E, which are calculated by Equation (8), Equation (9), and Equation (10), respectively.

$$I = \frac{d_{75} - d_{25}}{2d_{50}} \quad (8)$$

$$S = \frac{d_{25}}{d_{75}} \quad (9)$$

$$E = \frac{d_{75} - d_{25}}{2} \quad (10)$$

where d_{25} , d_{50} (cut particle size) and d_{75} are defined as the particle sizes corresponding to recoveries of 25%, 50% and 75% of the underflow on the efficiency curve.

In the evaluation of classification efficiency, the smaller the possible deviation E and imperfection I, and the larger the separation sharpness S, the higher the classification accuracy of the hydrocyclone (Ye et al., 2019; Liu et al., 2022). Table 3 shows the analysis results of the classification efficiency curve, the imperfection decreases and then increases with the increase of vane width, the separation sharpness shows the trend of increasing and then decreasing, and the vane width of 0.12D is the turning point of change. The width of the spiral vane is 0.04D, the hydrocyclone cutting particle size is the smallest, and the cutting particle size increases with the increase of the vane width. Moreover, with the width of the spiral vanes less than 0.12D, there is only a small difference in separation sharpness. Therefore, at the width of the spiral vane $C=0.04D$, the effect on fine particle classification is more favorable, and the underflow recovery of fine particles of 5 μm and 10 μm is reduced by 16.2% and 15.7%.

Table 3. Separation performance

Width of spiral vanes/mm	Cut size $d_{50}/\mu\text{m}$	Imperfection I	Sharpness of Separation S	Possible deviation E/ μm
0	26.7	0.363	0.466	9.69
3	26.4	0.340	0.498	9.00
6	27.1	0.333	0.506	9.02
9	27.5	0.331	0.509	9.10
12	27.7	0.361	0.476	10.00
15	29.1	0.389	0.450	11.31
18	31.8	0.451	0.403	14.36

4. Conclusions

By studying the flow field and separation performance of the hydrocyclone with spiral vanes, the appropriate width of the spiral vanes was determined to reduce the effect of entrainment fine particles in underflow in the hydrocyclone. Simulations were performed using CFD techniques, and the author drew the following conclusions from this study.

(1) The diameter of the air core in the flow field of SV hydrocyclone is smaller, which reduces the kinetic energy loss of the gas during the operation of hydrocyclone, so SV hydrocyclone has lower pressure drop, and its pressure drop decreases with the increase of the width of the spiral vane.

(2) Spiral vanes make the hydrocyclone working fluid flow along the specified trajectory, the fluid has a certain support effect, so that the hydrocyclone outer swirling flow area fluid axial velocity is reduced. And the greater the width of the vane, the axial velocity reduction is more obvious. This helps to extend the effective residence time of particles in the hydrocyclone flow field.

(3) The spiral vanes of the SV hydrocyclone have a certain effect of inflow on the working fluid, and increasing the width of the spiral vanes can reduce the turbulence intensity of the flow field and make its internal flow field more stable. However, it will also lead to the increase of the hydrocyclone split ratio thus reducing the underflow yield.

(4) The downward resistance generated by the spiral vanes in the SV hydrocyclone has a more pronounced effect on the fine particles. In the range of spiral vane width 0.04D to 0.12D, the classification efficiency of 5 μ m and 10 μ m particles is not much different, but the classification efficiency of coarse particles decreases with the increase of vane width.

Acknowledgment

This research was funded by National Natural Science Foundation of China (22108159) and Natural Science Foundation of Shandong province, China (ZR2021QB068, ZR2020ME105).

References

- DUCZEK, S., DUVIGNEAU, F., GABBERT, U., 2016. *The finite cell method for tetrahedral meshes*. Finite Elements in Analysis and Design, 121, 18-32.
- DUNDAR, H., 2020. *Investigating the benefits of replacing hydrocyclones with high-frequency fine screens in closed grinding circuit by simulation*. Minerals Engineering, 148, 106212.
- HOU, D.X., CUI, B.Y., ZHANG, H., ZHAO, Q., JI, A.K., WEI, D.Z., FENG, Y.Q. 2021. *Designing the hydrocyclone with flat bottom structure for weakening bypass effect*. Powder Technology, 394, 724-734.
- HOU, D.X., CUI, B.Y., ZHAO, Q., WEI, D.Z., SONG, Z.G., FENG, Y.Q., 2021. *Research on the structure of the cylindrical hydrocyclone spigot to mitigate the misplacement of particles*. Powder Technology, 387, 61-71.
- HSIEH K.T., RAJAMANI K., 1988. *Phenomenological model of the hydrocyclone: Model development and verification for single-phase flow*. International Journal of Mineral Processing, 22(1-4), 223-237.
- ISHAK, K.E.H.K., AYOUB, M.A., 2019. *Predicting the Efficiency of the Oil Removal From Surfactant and Polymer Produced Water by Using Liquid-Liquid Hydrocyclone: Comparison of Prediction Abilities Between Response Surface Methodology and Adaptive Neuro-Fuzzy Inference System*. IEEE Access, 7, 179605-179619.
- JE, Y.W., KIM, Y.J., KIM, Y.J., 2022. *The Prediction of Separation Performance of an In-Line Axial Oil-Water Separator Using Machine Learning and CFD*. Processes, 10(2), 375.
- JIANG, L.Y., LIU, P.K., YANG, X.H., ZHANG, Y.K., LI, X.Y., ZHANG, Y.L., WANG, H., 2020. *Experimental research on the separation performance of W-shaped hydrocyclone*. Powder Technology, 372, 532-541.
- JIANG, L.Y., LIU, P.K., ZHANG, Y.K., LI, X.Y., YANG, X.H., XU, H.L., WANG, H., 2022. *Experimental study of the separation performance of a hydrocyclone with a compound curve cone*. Powder Technology, 409, 117829.
- JING, J.Q., ZHANG, S.J., QIN, M., LUO, J.Q., SHAN, Y.T., CHENG, Y.Z., TAN, J.T., 2021. *Numerical simulation study of offshore heavy oil desanding by hydrocyclones*. Separation and Purification Technology, 258, 118051.
- JUNG, K.J., HWANG, I.J., KIM, Y.J., 2019. *Effect of inner wall configurations on the separation efficiency of hydrocyclone*. Journal of Mechanical Science and Technology, 33(11), 5277-5283.
- KOU, J., CHEN, Y., WU, J.Q., 2020. *Numerical study and optimization of liquid-liquid flow in cyclone pipe*. Chemical Engineering and Processing-Process Intensification, 147, 107725.
- KUANG, S.B., CHU, K.W., YU, A.B., VINCE, A., 2012. *Numerical study of liquid-gas-solid flow in classifying hydrocyclones: Effect of feed solids concentration*. Minerals Engineering, 31, 17-31.
- LEE, W., JUNG, M., HAN, S., PARK, S., PARK, J.K., 2020. *Simulation of layout rearrangement in the grinding/classification process for increasing throughput of industrial gold ore plant*. Minerals Engineering, 157, 106545.
- LI, C.Y., LI, J.P., WANG, N.N., ZHAO, Q., WANG, P., 2021. *Status of the treatment of produced water containing polymer in oilfields: A review*. Journal of Environmental Chemical Engineering, 9(4), 105303.
- LIU, P.K., FU, W.X., JIANG, L.Y., YANG, X.H., ZHANG, Y.K., LI, X.Y., ZHANG, Y.L., 2023. *Effect of the Position of Overflow Pipe with Mixed Spiral Structures on the Separation Performance of Hydrocyclones*. Separations, 10(2), 84.
- LIU, P.K., FU, W.X., JIANG, L.Y., ZHANG, Y.K., LI, X.Y., YANG, X.H., CHEN, B., 2022. *Effect of back pressure on the separation performance of a hydrocyclone*. Powder Technology, 409, 117823.
- LIU, B., LI, L.C., WANG, H.J., ZHAO, Z.J., QI, Y.G., 2020. *Numerical simulation and experimental study on internal and external characteristics of novel Hydrocyclones*. Heat and Mass Transfer, 56(6), 1875-1887.
- MOKNI, I., DHAOUAD, H., BOURNOT, P., MHIRI, H., 2015. *Numerical investigation of the effect of the cylindrical height on separation performances of uniflow hydrocyclone*. Chemical Engineering Science, 2015, 122, 500-513.
- MURTHY, Y.R., BHASKAR, K.U., 2012. *Parametric CFD studies on hydrocyclone*. Powder Technology, 230, 36-47.

- PADHI, M., KUMAR, M., MANGADODDY, N., 2020. *Understanding the Bicomponent Particle Separation Mechanism in a Hydrocyclone Using a Computational Fluid Dynamics Model*. *Industrial & Engineering Chemistry Research*, 59(25), 11621-11644.
- PADHI, M., MANGADODDY, N., SREENIVAS, T., VAKAMALLA, T.R., MAINZA, A.N., 2019. *Study on multi-component particle behaviour in a hydrocyclone classifier using experimental and computational fluid dynamics techniques*. *Separation and Purification Technology*, 229, 115698.
- PATRA, G., VELPURI, B., CHAKRABORTY, S., MEIKAP, B.C., 2017. *Performance evaluation of a hydrocyclone with a spiral rib for separation of particles*. *Advanced Powder Technology*, 28(12), 3222-3232.
- PATRA, G., BARNWAL, R., BEHERA, S.K., MEIKAP, B.C., 2018. *Removal of dyes from aqueous solution by sorption with fly ash using a hydrocyclone*. *Journal of Environmental Chemical Engineering*, 6(4), 5204-5211.
- QIU, S.Z., WANG, T., WANG, G.R., ZHONG, L., FANG, X., 2023. *Effect of Spiral Inlet Geometric Parameters on the Performance of Hydrocyclones Used for In Situ Desanding and Natural Gas Hydrate Recovery in the Subsea*. *ACS Omega*, 2023, 8(6), 5426-5436.
- SONG, T., YAO, Y., NI, L., 2020. *Response surface method to study the effect of conical surface and vortex-finder lengths on de-foulant hydrocyclone with reflux ejector*. *Separation and Purification Technology*, 253, 117511.
- SU, T.L., ZHANG, Y.F., 2022. *Effect of the Vortex Finder and Feed Parameters on the Short-Circuit Flow and Separation Performance of a Hydrocyclone*. *Processes*, 10(4), 771.
- TIAN, J.Y., NI, L., SONG, T., ZHAO, J.N., 2020. *CFD simulation of hydrocyclone-separation performance influenced by reflux device and different vortex-finder lengths*. *Separation and Purification Technology*, 233, 116013.
- VAKAMALLA, T.R., MANGADODDY, N., 2019. *The dynamic behaviour of a large-scale 250-mm hydrocyclone: A CFD study*. *Asia-Pacific Journal of Chemical Engineering*, 14(2), e2287.
- VEGA-GARCIA, D., BRITO-PARADA, P.R., CILLIERS, J.J., 2018. *Optimising small hydrocyclone design using 3D printing and CFD simulations*. *Chemical Engineering Journal*, 350, 653-659.
- VYSYARAJU, R., PUKKELLA, A.K., 2022. *Subramanian, S. Computational investigation of a novel hydrocyclone for fines bypass reduction*. *Powder Technology*, 395, 501-515
- WANG, W.Q., LIU Z.B., YANG F., 2023. *Enrichment and Recovery of Lead-Zinc Tailings by Spiral Wall Cyclones*. *Academic Journal of Architecture and Geotechnical Engineering*, 5, 14-20.
- XIE, H.Y., SUN, R., REN, X.J., YOU, Z.C., LIU, Y.H., FENG, D.X., CHEN, L.Z., 2020. *Development of a novel fluidized hydrocyclone concentrator for mineral separation*. *Separation and Purification Technology*, 248, 116960.
- XING, L., JIANG, M.H., ZHAO, L.X., GAO, J.M., LIU, L., 2022. *Design and analysis of de-oiling coalescence hydrocyclone*. *Separation Science and Technology*, 57(5), 749-767.
- YANG, X.H., YANG, G.H., LIU, P.K., LI, X.Y., JIANG, L.Y., ZHANG, J.S., 2022. *Study on the Desliming Performance of a Novel Hydrocyclone Sand Washer*. *Separations*, 9(3), 74.
- YE, Q., DUAN, P.B., KUANG, S.B., JI, L., ZOU, R.P., YU, A.B., 2022. *Multi-objective optimization of hydrocyclone by combining mechanistic and data-driven models*. *Powder Technology*, 407, 117674.
- YE, J.X., XU, Y.X., SONG, X.F., YU, J.G., 2019. *Numerical modelling and multi-objective optimization of the novel hydrocyclone for ultra-fine particles classification*. *Chemical Engineering Science*, 207, 1072-1084.
- ZHANG, H., NI, H.J., 2022. *Design and Numerical Simulation on New Type Near-Bit Hydrocyclone for Downhole Solid-Liquid Separation*. *Arabian Journal for Science and Engineering*, 47(9), 11941-11951.
- ZHANG, Y.J., QIAN, J., 2012. *Resolving topology ambiguity for multiple-material domains*. *Computer Methods in Applied Mechanics and Engineering*, 247, 166-178.
- ZHANG, C., WEI, D.Z., CUI, B.Y., LI, T.S., LUO, N., 2016. *Effects of curvature radius on separation behaviors of the hydrocyclone with a tangent-circle inlet*. *Powder Technology*, 305, 156-165.
- ZHAO, Z.J., ZHOU, L., LIU, B., CAO, W.D., 2022. *Computational fluid dynamics and experimental investigation of inlet flow rate effects on separation performance of desanding hydrocyclone*. *Powder Technology*, 402, 117363.
- ZHOU, M., FARKAS, L.A., KOKKILIC, O., LANGLOIS, R., ROWSON, N.A., WATERS, K.E., 2023. *An investigation into processing fine magnetite using a magnetic hydrocyclone*. *Canadian Metallurgical Quarterly*, 62(3), 497-501.
- ZHOU, F.Q., SUN, G.G., HAN, X.P., ZHANG, Y., BI, W.Q., 2018. *Experimental and CFD study on effects of spiral guide vanes on cyclone performance*. *Advanced Powder Technology*, 29(12), 3394-3403.